chemistry

MDPI

Article

Exploring the Structural Chemistry of Pyrophosphoramides: N,N′,N″,N‴-Tetraisopropylpyrophosphoramide

Duncan Micallef, Liana Vella-Zarb and Ulrich Baisch *

Department of Chemistry, Faculty of Science, University of Malta, MSD2080 Msida, Malta; duncan.micallef.11@um.edu.mt (D.M.); liana.vella-zarb@um.edu.mt (L.V.-Z.)
* Correspondence: ulrich.baisch@um.edu.mt; Tel.: +356-2340-3425

Abstract: N,N′,N″,N‴-Tetraisopropylpyrophosphoramide **1** is a pyrophosphoramide with documented butyrylcholinesterase inhibition, a property shared with the more widely studied octamethylphosphoramide (Schradan). Unlike Schradan, **1** is a solid at room temperature making it one of a few known pyrophosphoramide solids. The crystal structure of **1** was determined by single-crystal X-ray diffraction and compared with that of other previously described solid pyrophosphoramides. The pyrophosphoramide discussed in this study was synthesised by reacting iso-propyl amine with pyrophosphoryl tetrachloride under anhydrous conditions. A unique supramolecular motif was observed when compared with previously published pyrophosphoramide structures having two different intermolecular hydrogen bonding synthons. Furthermore, the potential of a wider variety of supramolecular structures in which similar pyrophosphoramides can crystallise was recognised. Proton (^{1}H) and Phosphorus 31 (^{31}P) Nuclear Magnetic Resonance (NMR) spectroscopy, infrared (IR) spectroscopy, mass spectrometry (MS) were carried out to complete the analysis of the compound.

Keywords: N,N,′N′′,N′′′-Tetraisopropylpyrophosphoramide; pyrophosphoramide; synthons; supramolecular motifs; X-ray crystallography

Citation: Micallef, D.; Vella-Zarb, L.; Baisch, U. Exploring the Structural Chemistry of Pyrophosphoramides: N,N′,N″,N‴-Tetraisopropylpyrophosphoramide. *Chemistry* **2021**, *3*, 13. https://doi.org/10.3390/chemistry3010013

Received: 20 December 2020
Accepted: 18 January 2021
Published: 28 January 2021

1. Introduction

N,N,′N′′,N′′′-Tetraisopropylpyrophosphoramide **1** ($O((iPrNH)_2PO)_2$) is a commercially available pyrophosphoramide known to be a butyrylcholinesterase inhibitor [1,2]. Although the molecular structure of the compound is known, crystallographic support for this structure has not been published. Another pyrophosphoramide that has shown cholinesterase inhibition is octamethylpyrophosphoramide ($O(Me_2N)_2PO)_2$), which is commonly known as Schradan. This compound, unlike **1**, was used as an insecticide for sucking and chewing insects, which are agricultural pests but it has fallen out of use since the 1950's [3,4]. Schradan is a liquid at room temperature making its storage, use, and structural characterisation more problematic than **1**. In the mid-twentieth century, apart from its use as a pesticide, Schradan was also studied for its chelation ability with numerous metal centres. These studies mainly dealt with the complexation of Schradan with alkali earth, transition and actinide metals, as well as Sn^{4+} [5–9]. Although the complexation ability was proven through numerous analytical methods, including X-Ray diffraction (XRD), no industrial or chemical use for these complexes was discussed. Only six other analogues of pyrophosphoramides were found in the literature, namely N,N′,N″,N‴-Tetrakis(2-methylphenyl)- oxybis(phosphonic diamide) ($O((2\text{-}MePh)NH)_2PO)_2$), N,N′,N″,N‴-tetra-tert-butoxybis(phosphonic diamide) ($O((tBuNH)_2PO)_2$), N,N′,N″,N‴-tetrakis(4-methylphenyl)-oxybis(phosphonic diamide) ($O((4\text{-}MePh)NH)_2PO)_2$), N,N′,N″,N‴-tetrakis(benzyl)-N,N′,N″,N‴-tetrakis(methyl)oxybis- (phosphonicdiamide)

($O((BzMeN)_2PO)_2$), 2,2′-Oxybis(1,3-bis(2,6-diisopropylphenyl)-1,3,2-diaza -phospholidine) 2,2′-dioxide ($O((C_2H_4(2,5\text{-}i\text{PrPhN})_2)_2PO)_2$) and 2,2′-oxybis(1,3-bis-[(naphthalen-1-yl)methyl]octahydro-1H-1,3,2λ⁵-benzodiazaphosphol-2-one) monohydrate ($O((1,2\text{-}Cy(NaphN)_2)_2PO)_2 \cdot H_2O$) [10–15].

These solids were characterised by single-crystal X-ray diffraction (SXRD) and published as novel structures with little detailed discussion on any similarities in structure and chemistry as opposed to the research carried out on Schradan. The latter two of the four were compared as part of a Hirshfeld analysis for phosphoramides. $O((t\text{BuNH})_2PO)_2$ was complexed with manganese(II) to give the complex $[Mn(O(t\text{BuNH})_2PO)_2)_2DMF_2][Cl]_2 \cdot 2H_2O$ [16]. This was the only published non-Schradan complex of this group of analogous pyrophosphoramides.

The main objective of this work was to study the supramolecular features of **1** and other, already published, pyrophosphoramides in light of known intermolecular interactions and arrangements [17–21] and to understand their influence on the physical properties of these compounds.

2. Materials and Methods

2.1. General Considerations

All reactions were carried out under an argon atmosphere using Schlenk line techniques. Chloroform was dried over a P_2O_5 still, while diethyl ether, THF, petroleum ether and chloroform used in the work-up procedures of the product were dried over 4 Å molecular sieves. FT-IR (Fourier Transform Infrared) spectra were recorded using KBr pellet samples and a Shimadzu IRAffinity-1 FTIR spectrophotometer. ^{1}H NMR and ^{31}P NMR (Nuclear Magnetic Resonance) spectra were collected on a Bruker Ascend NMR spectrometer with a probe having a set frequency of 500.13 MHz for ^{1}H NMR and 202.457 MHz for ^{31}P NMR. Gas chromatography Mass spectroscopy (GC MS) data was collected using a Thermo DSQ II GC/MS spectrometer with samples being prepared by dissolution of the products in chloroform. Single-crystal X-ray diffraction data was collected on a STOE STADIVARI diffractometer.

2.2. Synthesis of N,N′,N″,N‴-Tetraisopropylpyrophosphoramide ($O((i\text{PrNH})_2PO)_2$)

The synthesis of $O((i\text{PrNH})_2PO)_2$ **1** was performed through a modification of the synthesis of the analogous $O((Me_2N)_2PO)_2$ (Schradan) as described by Goehring, M. and Niedenzu, K. in 1956 [22]. Iso-propyl amine (5 mL, 0.058 mol) was dissolved in 10 mL of chloroform as a solvent. The mixture was cooled to −78 °C and pyrophosphoryl tetrachloride (1 mL, 0.007 mol) was added dropwise to the reaction solution using a glass syringe. Upon addition of pyrophosphoryl tetrachloride, the formation of white fumes was noted, along with the formation of a solid crystalline mass. The reaction was left at a temperature of -78 °C until the white fumes dissipated and was subsequently allowed to reach room temperature. The reaction mixture was left to react at room temperature overnight. The white suspension thus formed was subsequently heated to 60 °C for 3 h to complete the reaction. The yellow solution obtained was left overnight to form a clear colourless crystalline mass ($i\text{PrNH}_3Cl$). The mixture was then filtered to collect a clear colourless crystalline mass ($i\text{PrNH}_3Cl$) and a yellow solution. The latter was layered with diethyl ether to yield a white solid. Yield, 41% (crude product with respect to pyrophosphoryl tetrachloride), ^{1}H NMR ($CDCl_3$): 8.31 ppm (s, 1H, NH3), 3.64 ppm (td, 1H, CH), 3.40 ppm (m, 1H, CH), 2.26 ppm (s, 1H, NH), 1.39 ppm (d, 2H, CH3) and at 1.14 ppm (t, 6H, CH3), ^{31}P {^{1}H} NMR ($CDCl_3$): 14.33 ppm (s), FT-IR (KBr, cm^{-1}): 3400 (w), 3252 (sb), 2965 (s), 2870 (m), 1637 (m), 1527 (m), 1466 (m), 1432 (m), 1396 (m), 1367 (m), 1257 (s), 1229 (s), 1167 (m), 1137 (w), 1055 (s), 1026 (s), 945 (m), 914 (m), 886 (s), 804 (m), 750 (m), GC MS (EI; 70 eV) *m*/*z*: 44.12, 58.08, 79.01, 93.97, 137.07, 179.10 $[(i\text{PrNH})_2PO_2]^+$, 195.16.

Crystals suitable for SXRD studies were obtained through liquid–liquid diffusion crystallisation: A sample of the white solid product was dissolved in a minimum volume

of chloroform to yield a saturated solution. This was layered with 30–40 °C petroleum ether in a 1:5 volume ratio of chloroform/petroleum ether. This produced a liquid-liquid diffusion crystallisation set up which yielded a white crystalline solid over the course of two days. The solid was collected by cannula filtration and crystals suitable for SXRD studies were collected from this solid.

2.3. Purification by Column Chromatography

Although single crystals of O((*i*PrNH)$_2$PO)$_2$ were obtained from the product, it is evident from NMR and GC MS data that this solid was not pure and therefore a sample of O((*i*PrNH)$_2$PO)$_2$ was also purified by column chromatography to determine whether this was a possible method of purification. The sample was dissolved in dichloromethane and activated Keiselgel 60 was used as the stationary phase, while THF/acetonitrile (1:1 *v*/*v*) was used as a mobile phase. ^{1}H NMR ($CDCl_3$): 3.37 (m, 1H, CH), 2.29 (bt, 1H, NH), 1.16 (t, 6H, CH_3), ^{31}P {^{1}H} NMR ($CDCl_3$): 14.33 ppm (s), FT-IR (KBr, cm^{-1}): 3414 (w), 3255 (bm), 2965 (s), 2870 (m), 1465 (m), 1428 (m), 1367 (m), 1257 (s), 1205 (s), 1167 (m), 1137 (m), 1051 (s), 1021 (s), 916 (m), 886 (m), 833 (sh), 800 (vw), 771 (m), GC MS (EI; 70 eV) *m*/*z*: 44.12, 58.11, 79.01, 93.93, 137.09, 179.10 [(iPrNH)$_2$PO$_2$]$^+$, 195.16.

2.4. Single-Crystal X-Ray Diffraction

Crystals were collected under oil and mounted in oil. Data was collected using Cu radiation on a STOE STADIVARI diffractometer, using a 200 K Pilatus detector at 293 K. The ShelXT intrinsic phasing method and ShelXL least squares method were used for structure solution and refinement, respectively (Table 1, Figure 1 and 2). Details regarding the structure solution and refinement procedures are described in Appendix A, while further detailed structural information for this structure is given in Tables S5–S9 in the Supplementary Materials.

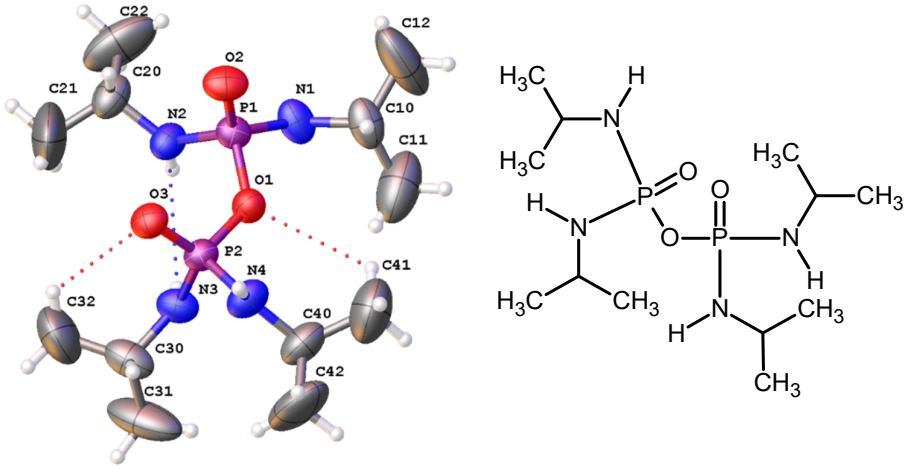

(**a**) (**b**)

Figure 1. (**a**) Molecular structure obtained for O((*i*PrNH)$_2$PO)$_2$ the hydrogen bonding N3–H1···N2 (blue) and the weak hydrogen bonding observed as C32–H32A···O3 and C41–H41A···O1 (red)(generated using Olex2 [23]); (**b**) molecular diagram for O((*i*PrNH)$_2$PO)$_2$ (generated using ChemSketch [24]).

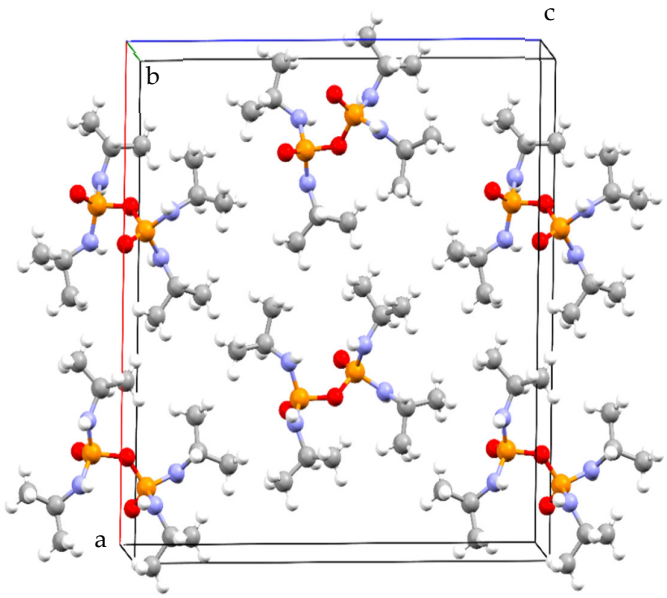

Figure 2. Unit cell for O((*i*PrNH)$_2$PO)$_2$ viewed along the b-axis (generated in Mercury [25]).

Table 1. Crystal data and structure refinement for O(*i*PrNH)$_2$PO)$_2$.

Empirical formula	$C_{12}H_{32}N_4O_3P_2$	μ/mm^{-1}	2.133
Formula weight/gmol^{-1}	342.35	F(000)	744.0
Temperature/K	293	Crystal size/mm^3	0.8 × 0.6 × 0.3
Crystal system	orthorhombic	Radiation	CuKα (λ = 1.54186)
Spacegroup	*Pca*2$_1$	2Θ range for data collection/°	8.696 to 137.268
a/Å	20.342(2)	Index ranges	−24 ≤ h ≤ 23, −3 ≤ k ≤ 6, −20 ≤ l ≤ 23
b/Å	5.0495(6)	Reflections collected	43032
c/Å	19.103(3)	Independent reflections	3317 [Rint = 0.0557, Rsigma = 0.0226]
α/°	90	Data/restraints/parameters	3317/1/214
β/°	90	Goodness-of-fit on F2	1.044
γ/°	90	Final R indexes [I > =2σ (I)]	R1 = 0.0402, wR2 = 0.1071
Volume/Å^3	1962.2(4)	Final R indexes [all data]	R1 = 0.0408, wR2 = 0.1075
Z	4	Largest diff. peak/hole/eÅ^{-3}	0.28/−0.29
ϱ calc/gcm^{-3}	1.159	Flack parameter	0.01(3)

3. Results and Discussion

3.1. Structural Comparison with Previously Described Pyrophosphoramides

Most intermolecular motifs that build up the supramolecular structure of a compound are due to the moieties within the molecule in question. Therefore, compounds with similar moieties and chemical structures may be expected to have similar intermolecular motifs and in turn, similar crystal structures [17,18]. In this regard, the

various pyrophosphoramides discussed in this study can be divided into five main groups, dependent on their chemical structure (Table 2).

Table 2. Categorisation of pyrophosphoramides discussed in this publication including crystal structures and space groups published from data obtained by single-crystal X-ray diffraction for the solid products, along with the liquid $O((Me_2N)_2PO)_2$.

Pyropshophoramides				
Di-N-Substituted Pyrophosphoramides			**Mono-N-Substituted Pyrophosphoramides**	
$O((R_2N)_2PO)_2$ (Symmetric secondary amine)	$O((R^1R^2N)_2PO)_2$ (Asymmetric secondary amine)	$O((R^1(NR^2)_2)_2PO)_2$ (N,N′-substituted diamine derivatives)	$O((AlkylNH)_2PO)_2$ (Primary alkyl amine derivatives)	$O((ArlyNH)_2PO)_2$ (Primary aryl amine derivatives)
$O((Me_2N)_2PO)_2$ Liquid [3,4]	$O((BzMeN)_2PO)_2$ *C2/c* [13]	$O((C_2H_4(2,5\text{-}i\text{PrPhN})_2)_2PO)_2$ *P2₁/n* [14]	$O((t\text{BuNH})_2PO)_2$ *P2₁/c* [12]	$O((2\text{-}MePhNH)_2PO)_2$ *P2₁/c* [10,11]
		$O((1,2\text{-}Cy(NaphN)_2)_2PO)_2$ *C2* [15]	$O((i\text{PrNH})_2PO)_2$ *Pca2₁* (current)	$O((4\text{-}MePhNH)_2PO)_2$ *Pccn* [13]

On comparison of the crystal structures of the compounds classified in each group, the most important molecular difference that seemed to affect the supramolecular structure was the presence of the N–H moiety. Its presence caused a significant difference between the structure of the mono-N-substituted pyrophosphoramides and the di-N-substituted pyrophosphoramides, which lack this moiety. In the crystal structures of mono-N-substituted pyrophosphoramides P=O···H–N hydrogen bonds were the most prominent and common intermolecular bonds in the structure. These formed numerous intermolecular and intramolecular synthons, which were the primary cause for the formation of the various supramolecular motifs observed, and which dictated both structure and symmetry [17–19]. The di-N-substituted pyrophosphoramides were shown to form crystalline structures wherein the pyrophosphoramide moieties did not interact with each other directly. Thus, no strong intermolecular interactions were found. The organic moieties therefore had a significant impact on the packing of molecules in the crystal structures obtained in contrast to the mono-N-substituted pyrophosphoramides (Table 3).

Table 3. Hydrogen bond distances in the crystal structure of **1.**

D	H	A	d(D-A)/Å	d(H-A)/Å	d(D-A)/Å	D-H-A/°
C41	H41A	O1	0.96	2.99	3.601(11)	122.9
C42	H42B	O2 [1]	0.96	2.58	3.505(8)	161.4
C32	H32A	O3	0.96	2.85	3.511(10)	126.4
N3	H3	O3 [2]	0.75(5)	2.34(5)	3.063(4)	164(5)
N3	H3	N2	0.75(5)	2.98(5)	3.491(5)	128(4)
N1	H1	O2 [2]	0.70(4)	2.22(4)	2.907(4)	170(5)
N4	H4	N3 [3]	0.92(6)	2.79(6)	2.979(4)	161(5)
N2	H2	O3 [2]	0.85(6)	2.16(6)	2.979(4)	161(5)

[1] 3/2-X,+Y,1/2+Z; [2] +X,-1+Y,+Z; [3] +X,1+Y,+Z.

3.1.1. Structural Comparison of mono-N-substituted pyrophosphoramides.

Given that the compound characterised in this current study, **1**, was a mono-N-substituted pyrophosphoramide its novel structure is best discussed in relation to other mono-N-substituted pyrophosphoramides. Despite its chemical similarities to $O((t\text{BuNH})_2PO)_2$, it not only crystallised in a different spacegroup, namely *Pca2₁*, but it

also showed a different supramolecular motif. First, the already published structures will be discussed and then compared with **1**.

The structures of Mono-N-substituted pyrophosphoramides $O((RNH)_2PO)_2$ were found to crystallise in two space groups: either $P2_1/c$ or *Pccn*. Common supramolecular arrangements form part of the crystal structures of $O((t\text{BuNH})_2PO)_2$ and the two $O((2\text{-MePhNH})_2PO)_2$ polymorphs [10–12] (Figure 3). The first one is a ring synthon with a $R_2^2(8)$ graph set binding molecules through intermolecular hydrogen bonding, while in the other [17,19] a partially eclipsed conformations is reached (Figure 3). The second synthon constricts the molecules from taking on other conformations and therefore minimises the number of possible supramolecular structures available. These two synthons together create the same supramolecular structure for all of the above crystal structures, namely a chain like packing as given in Figure 4. The respective structures for the three mono-N-substituted pyrophosphoramides are shown in Figure 5. This structure motif is repeated through translational symmetry to form infinite chains. The two molecules that form the actual supramolecular units are related to each other by the glide plane denoted in the $P2_1/c$ spacegroup.

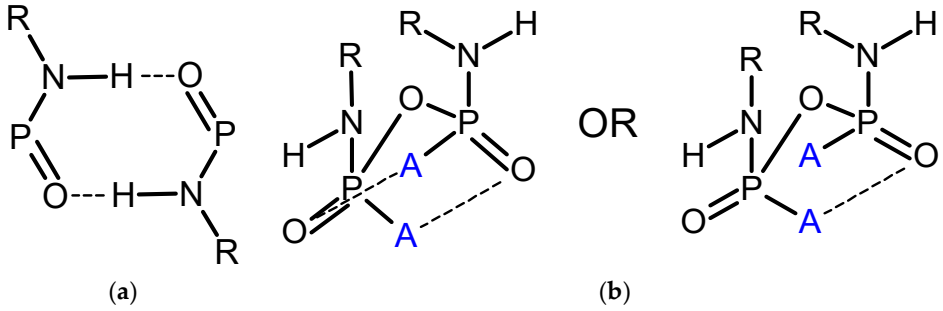

Figure 3. H-bonding synthons in $P2_1/c$ structures: (**a**) intermolecular ring synthon; (**b**) the two variants of the intramolecular synthon where A is the non-intermolecular bonding amine (all generated using ChemSketch [24]).

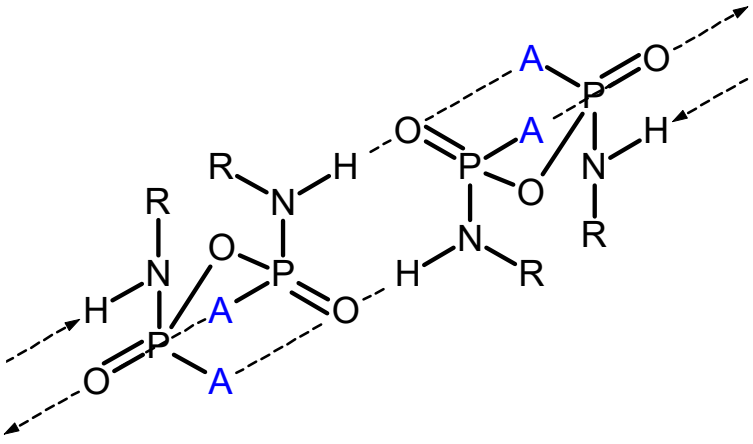

Figure 4. Basic unit for the supramolecular H-bonding motif that is common to all three mono-N-substituted pyrophosphoramides crystallising in $P2_1/c$ (generated using ChemSketch [24]).

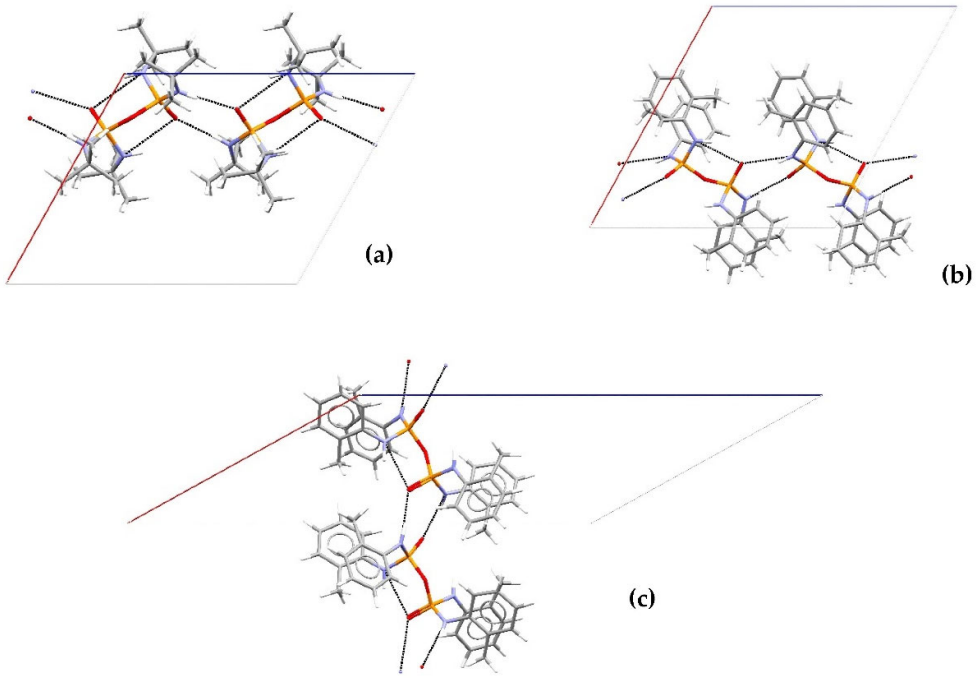

Figure 5. The hydrogen bonding motif common to all $P2_1/c$ as noted in the published structures: (**a**) O((*t*BuNH)$_2$PO)$_2$; (**b**) O((2-MePhNH)$_2$PO)$_2$ published by Pourayoubi et al. [11]; (**c**) O((2-MePhNH)$_2$PO)$_2$ published by Cameron et al. [10] (all generated in Mercury [25]).

Formation of this hydrogen bonding motif seems to be independent of the nature of the organic substituent on the amide nitrogen, as it occurs for both the alkyl tert-butyl and aryl 2-methylphenyl analogues. The packing of these chains is, however, influenced by the organic substituents. The tert-butyl groups in O((*t*BuNH)$_2$PO)$_2$ pack in a staggered formation resulting in the closest possible packing of the chains [12]. No additional intermolecular interactions are detected within the usual limits.

The packing effects of the 2-methylphenyl groups are more complex than those of the tert-butyl groups. They give rise to two polymorphs of this compound. The two molecular components of these supramolecular units are related to each other by the glide plane imposed by the $P2_1/c$ spacegroup. In the two O((2-MePhNH)$_2$PO)$_2$ polymorphs however, the direction of the motif is different. The motif in the polymorph reported by Pourayoubi, M. et al. is built along the *c* axis while the same motif in the polymorph described by Cameron, S.T. et al. is perpendicular to the *c* axis. Given that the hydrogen bond interaction is identical in both polymorphs, the difference lies in the way the supramolecular chains pack. The polymorph discussed by Pourayoubi et al. [11] showed closer packing between the chains. In both polymorphs the 2-methylphenyl groups are oriented antiparallel to each other (Figures 6 and 7). The stacking distances between the intramolecular 2-methylphenyl moieties are 3.539 Å and 3.933 Å [10,11]. In one polymorph [11] the position of the chains seems mainly influenced by the supramolecular structure given in the diagram shown in Figure 6. A square like motif is formed wherein each side is composed of the Ph(π)···H–C(meta) interactions [17]. Two contact distances of 3.159 Å and 3.188 Å are present, which are shorter than any contact distance reported in the polymorph described by Cameron et al. [10]. The latter forms similar inter- and intramolecular interactions with one much larger contact distances of 4.717 Å and a very oblique interaction between neighbouring molecules, not bound by hydrogen bonding, with a distance of 3.626 Å [10]. The former interaction is longer than any interactions described for the other polymorph and indicates a less efficient packing. Thus, the

different modes of packing of the organic moieties are most probably the cause of the formation of the two polymorphs.

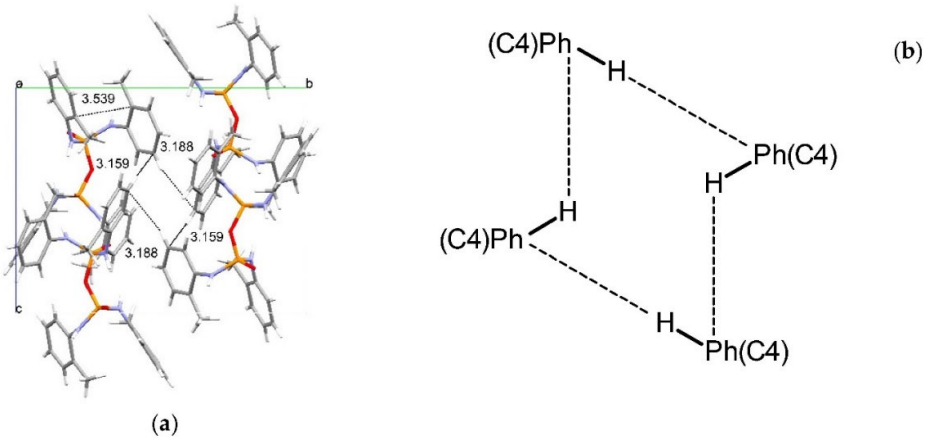

Figure 6. (**a**) $O((2\text{-}MePhNH)_2PO)_2$ polymorph published by Pourayoubi et al. showing both intermolecular and intramolecular C–H···Ph interactions (generated in Mercury [25]); (**b**) a diagram of the intermolecular C–H···Ph interactions for clarity (generated using ChemSketch [24]).

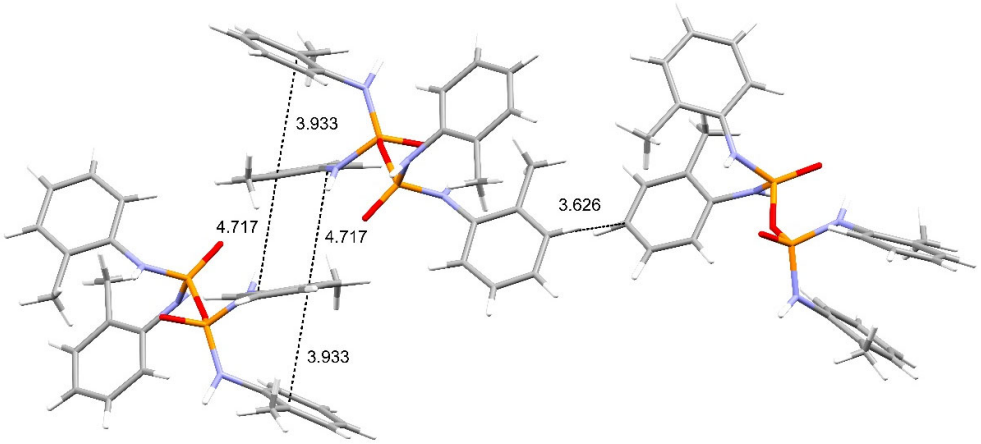

Figure 7. $O((2\text{-}MePhNH)_2PO)_2$ polymorph published by Cameron et al. showing both intermolecular and intramolecular C–H···Ph interactions (generated in Mercury [25]).

Experimental procedures on how to obtain only one of two polymorphs are not reported in the literature. The $O((2\text{-}MePhNH)_2PO)_2$ structure published by Cameron et al. was obtained by the reaction of phosphenyl chloride with ortho-methylaniline followed by recrystallisation in methanol. The synthesis of the polymorph obtained by Pourayoubi et al. was not described in the literature to the best of our knowledge. Interestingly, the crystallographic data of the two structures was collected at different temperatures (150K for [11] and 295K for [10,11]). It is, therefore, possible that a polymorphic transition occurs at lower temperatures. This is also in agreement with the difference in the corresponding unit cell volumes.

The mono-N-substituted pyrophosphoramides, which do not crystallise in the $P2_1/c$ spacegroup, show different inter- and intramolecular hydrogen bonding motifs. Given that the compounds crystallising in the same spacegroup ($P2_1/c$) contain both alkyl and aryl moieties and show a different packing of these moieties, a similar observation is expected for the 4-methylphenyl and the iso-propyl analogues. However, a different supramolecular structure was formed by the 4-methylphenyl derivative O((4-

MePhNH)$_2$PO)$_2$, crystallising in spacegroup *Pccn* [13]. There is no intramolecular synthon present (Figure 3b), resulting in a different pattern of supramolecular interactions. The phosphoryl oxygen and the amide nitrogen, which typically form the intramolecular P=O···H–N motif in the *P*2$_1$/*c* structures, do not show any hydrogen bonding and therefore, the molecules are not limited to an eclipsed conformation (*vide supra*). They form a staggered conformation that enables the formation of the basic supramolecular building block for this structure. Two molecules are connected via two intermolecular P=O···H–N hydrogen bonds, forming a ring synthon with graph set $R_2^2(12)$ (Figure 8) [13,19]. Further N–H···Ph and P=O···H–C(Ph(C2)) interactions are observed. The N–H···Ph interactions are formed through the remaining amide moieties which do not interact in the $R_2^2(12)$ ring described prior and this additional set of interactions seems to stabilise the motif by increasing the packing efficiency and stopping this moiety from forming the previously mentioned intramolecular P=O···H–N bonding. The P=O···H–C(Ph(C2)) interactions also seem to add stability by further aiding the P=O oxygen atoms to obtain the orientation necessary to form this synthon [17,21].

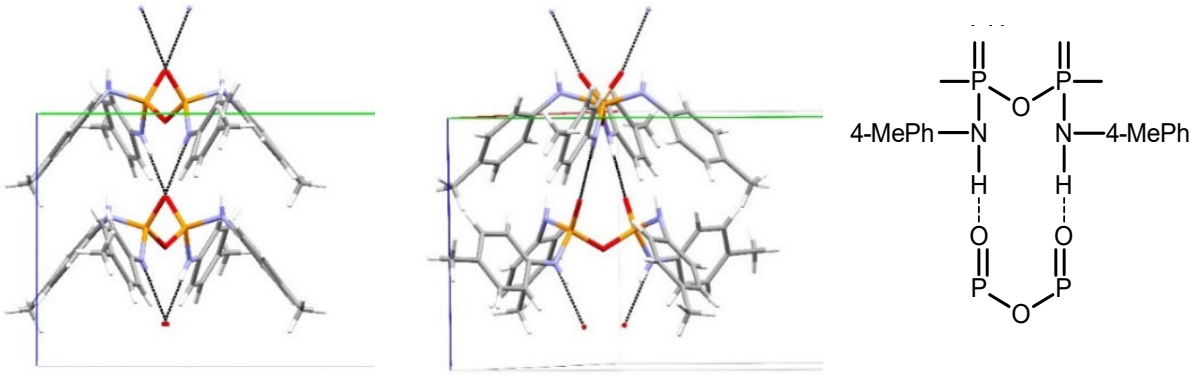

(**a**) (**b**)

Figure 8. Hydrogen bonding motif for O((4-MePhNH)$_2$PO)$_2$ (**a**) as viewed along the *a*-axis (**left**) and offset to show the staggered conformation of the pyrophosphoramide (**right**) (generated in Mercury [25]); (**b**) The ring synthon responsible for the motif given in a simplified diagram (generated using ChemSketch [24]).

The two molecules are related by a glide plane on the *a*-*c* plane along the *c* axis (Figure 9) which results in the formation of infinite chains along cell axis *c*. Neighbouring chains positioned anti-parallel to each other along the *b* axis and related to each other by a second glide plane along the diagonal of the *ab* plane. Chains neighbouring each other along the *a* axis are parallel and again related by translation. The main interaction responsible for arrangement in antiparallel chains is the Ph(π)···H–C(para-methyl) interaction between the closely situated 4-methyphenyl groups bound to different molecules in different chains [21], as noted in Figure 9 [13]. This guarantees the closest possible packing of the various phenyl groups in the molecule. Thus, the 4-methylphenyl groups seem to play a structure forming role in both the formation of a different hydrogen bonding motif and a different packing of the molecules in this structure compared to other pyrophosphoramides.

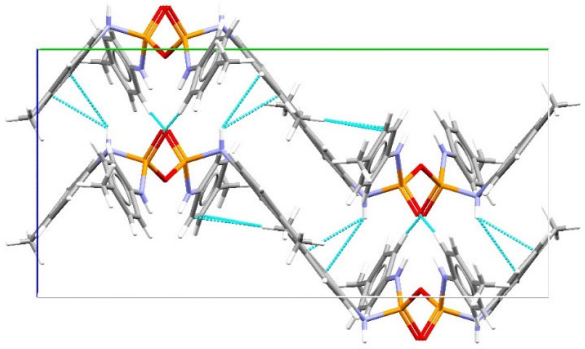

Figure 9. Intermolecular and intramolecular non-hydrogen bonding interactions in the structure of $O((4\text{-}MePhNH)_2PO)_2$ (generated in Mercury [25]).

The 2-methylphenyl and 4-methylphenyl derivatives both crystallise in different supramolecular structures and space groups. However, the 2-methylphenyl pyrophosphoramide crystallises in the same space group and shows the same supramolecular bonding as that for the tert-butyl analogue. $O((4\text{-}MePhNH)_2PO)_2$. The latter was collected at 90 K, whereas the $O((2\text{-}MePhNH)_2PO)_2$ polymorphs were collected at 150 K and 295 K [10,11,13]. Thus, it is unclear whether the occurrence of different structural motifs is mainly caused by the different nature of the side groups or simply because the single crystal data was collected for each compound at different temperatures

No intramolecular P=O···H–N hydrogen bonding is present in the crystal structure of **1**. This leads to the formation of a staggered arrangement of the pyrophosphoramide group similar to that observed for $O((4\text{-}MePhNH)_2PO)_2$. Thus again, the lack of intramolecular bonding between amide and phosphoroxide seems to hinder an eclipsed conformation (*vide supra*, Figure 3b) and related supramolecular motifs. The most important supramolecular motif in the structure of **1** is therefore the P=O···H–N interaction. This is in agreement with what was observed also in all other mono-N-substituted pyrophosphoramides, where intermolecular hydrogen bonding was a major factor in the formation of the relevant supramolecular motifs [10–13]. The actual synthon is shown in Figure 10. It is formed by two molecules of **1** related to each other by translation symmetry via two different P=O···H–N hydrogen bonding synthons. To the best of our knowledge this is the only mono-N-substituted pyrophosphoramide structure to exhibit multiple intermolecular hydrogen bonding synthons. The first synthon is a ring with a $R_2^1(8)$ graph set connecting one P=O group with two neighbouring N–H groups, which are bound to the two different phosphorus centres of the second molecule. The second synthon consists of a P=O···H–N interaction between the other P=O group of the first molecule and a neighbouring N–H group. The latter is not part of the previously discussed synthon; it shares, however, a phosphorus centre with one of the previously discussed amide groups. Neighbouring chains along the *a* axis pack anti-parallel to each other via a 2_1 screw axis (Figure 11). The remaining amide does not seem to participate in any type of intermolecular or intramolecular bonding, even though, theoretically, infinite chains along the *b* axis could be formed in a similar manner as observed in other mono-N-substituted pyrophosphoramides (*vide supra*). Therefore, the main mode of intermolecular interactions is the Van der Waals forces that caused the hydrophobic iso-propyl groups to stack.

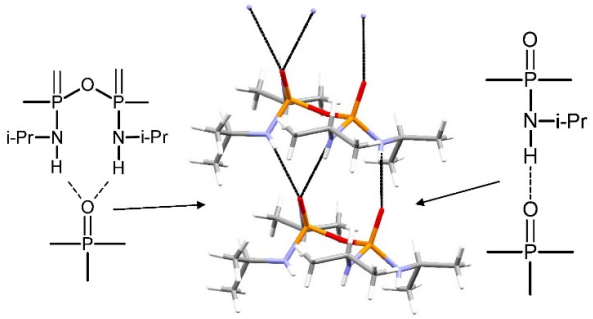

Figure 10. Hydrogen bonding synthons present in the structure of O((*i*PrNH)$_2$PO)$_2$ (generated in Mercury [25] and ChemSketch [24]).

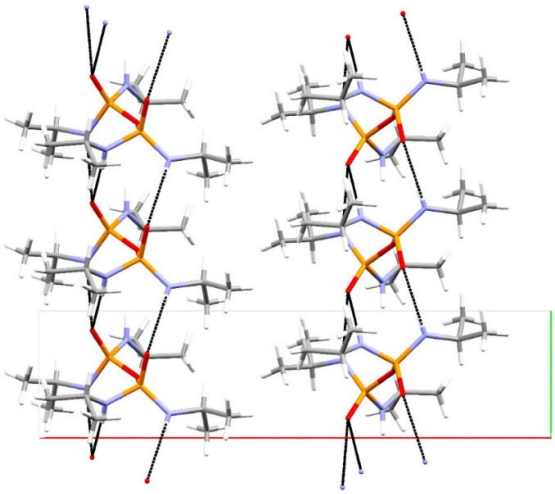

Figure 11. Antiparallel chains of O((*i*PrNH)$_2$PO)$_2$ noted along the a-axis (generated in Mercury [25]).

The cause for the formation of this different supramolecular motif is difficult to determine as the different molecular structure, synthesis, crystallisation techniques, and solvents used can all affect crystallization process and lead to this crystal structure. The temperature at which single crystal data was obtained is unlikely to be the cause of this as it falls into the same range as for the other compounds crystallising in spacegroup $P2_1/c$ [10–12]. The synthesis and crystallisation approach used to obtain single crystals of **1** differs from published procedures to obtain crystalline material for the related compounds . Given the chemical similarities between the iso-propyl and tert-butyl moiety the difference in supramolecular motifs between the two is unexpected.

3.1.2. Structural Comparison of di-N-Substituted Pyrophosphoramides

Because of the lack of a N-H donor in di-N-substituted pyrophosphoramides the main supramolecular interactions present in the crystal structure derive from the organic substituents. A very good and well-known example of a di-N-substituted pyrophosphoramide O((R$_2$N)$_2$PO)$_2$ is Schradan, O((Me$_2$N)$_2$PO)$_2$ [3–9,22]. Schradan is a liquid at room temperature. No crystal structures collected of crystals below the melting point temperature are reported in the literature. Structural information from experimental data is only available for O((R^{1}R^{2}N)$_2$PO)$_2$ and the N,N′-substituted diamine derivatives O((R^1(NR^2)$_2$)$_2$PO)$_2$, i.e., O((BzMeN)$_2$PO)$_2$, O((C$_2$H$_4$(2,5-*i*PrPhN)$_2$)$_2$PO)$_2$ and O((1,2-Cy(NaphN)$_2$)$_2$PO)$_2$ [13–15]. No significant classical intermolecular interactions between the pyrophosphoramide or organic moieties are present in the corresponding published crystal structures. The pyrophosphoramide backbone forms a similar staggered

conformation in all three compounds. In $O((BzMeN)_2PO)_2$, the main intermolecular interactions effecting the supramolecular structure are weak C–H···Ph interactions [13]. These form in two different synthons, namely N–Me···Ph(C2) and CH_2(benzyl)···Ph. The molecules pack in layers linked along the axis *c* (Figure 12) [17,21].

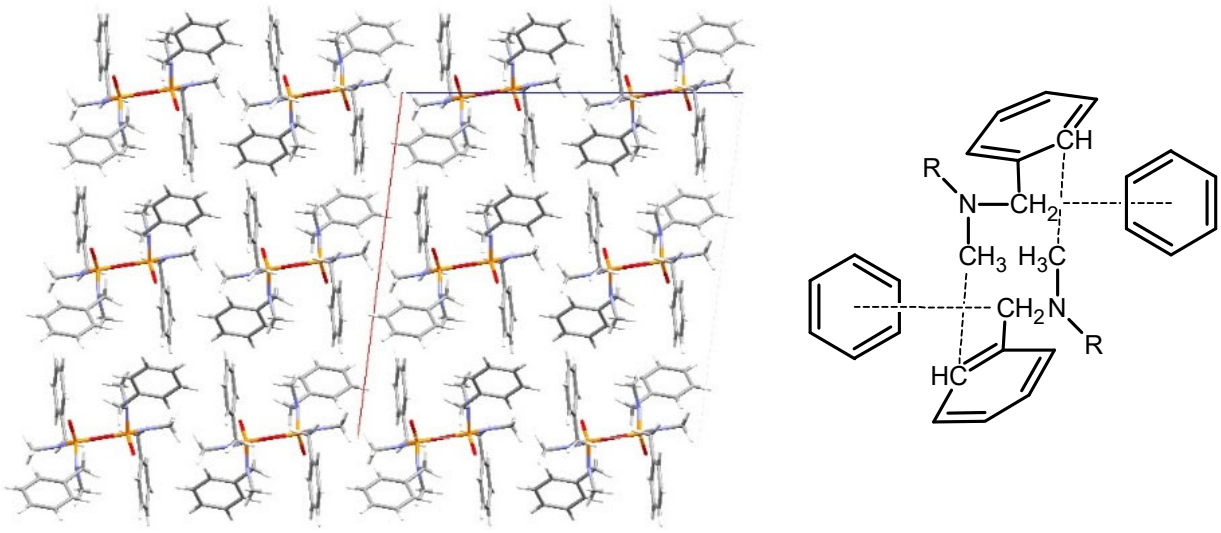

(**a**) (**b**)

Figure 12. Packing of $O((BzMeN)_2PO)_2$: (**a**) C–H···Ph interactions which act as the main supramolecular building block (generated in Mercury [25]); (**b**) simplified diagram of the supramolecular motif (generated using ChemSketch [24]).

The crystal structure of $O((C_2H_4(2,5\text{-}i\text{PrPhN})_2)_2PO)_2$ shows only very weak intermolecular interactions [14]. The pyrophosphoramide moieties seem to be isolated from each other by the bulky hydrophobic organic moieties (Figure 13).

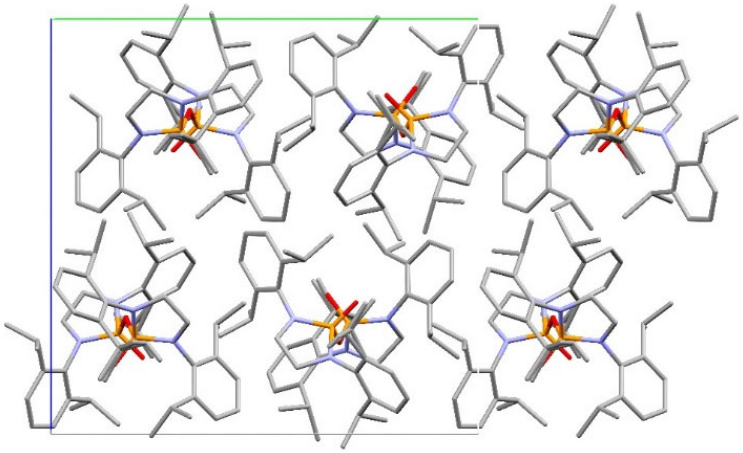

Figure 13. Structure of $O((C_2H_4(2,5\text{-}i\text{PrPhN})_2)_2PO)_2$ as viewed along the a-axis (generated in Mercury [25]).

In the crystal structure of $O((1,2\text{-Cy}(NaphN)_2)_2PO)_2$ intermolecular motifs (C–H···Ph interactions) are present similar to those observed in the structure of $O((BzMeN)_2PO)_2$. Intermolecular interactions are noted between the benzyl methylene, the naphthyl groups and the cyclohexyl –CH_2– groups. Three distinct C–H···Ph interactions are present namely CH_2(benzyl methylene)···naphthyl(C4), C–H(Naphthyl(C8))···naphthyl(C10) , and CH_2(cyclohexyl)···napthyl(C3) [15]. These interactions are unidirectional, with the proton donors binding to the closest naphthalene along the *c* axis, which is typically the molecule

diagonal to the proton donor molecule in the layers running along axis *a* (Figure 14). The pyrophosphoramide group is connected to hydrate water by hydrogen bonding forming a $R_2^2(8)$ ring [15]. This ring motif separates the pyrophosphoramide molecule structurally from any further interaction with typical hydrogen bonding electron acceptors.

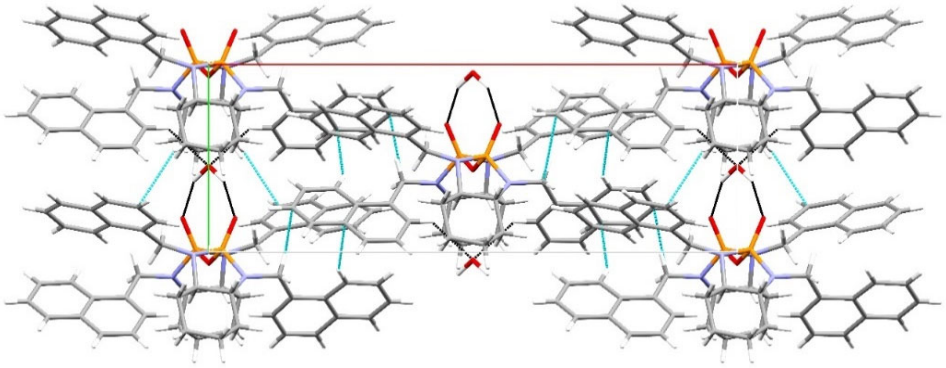

Figure 14. Structure of O((1,2-Cy(NaphN)$_2$)$_2$PO)$_2$ viewed along the c-axis showing hydrogen bonding (black contacts) and C–H···Ph interactions (light blue contacts) (generated in Mercury [25]).

In all three cases the supramolecular structure is dominated by the organic substituents. There is complete lack of π–π stacking interactions. A possible reason for this might be that the pyrophosphoramide backbone always takes on a more staggered conformation forcing the organic substituents into unfavorable positions to form π–π stacking. The staggered conformation itself is most likely caused by the lack of the amine N–H bonds, which usually force the molecule in a more eclipsed conformation through inter/intramolecular bonding as observed in some of the mono-N-substituted pyrophosphoramides.

4. Conclusions

The crystal structure of the mono-N-substituted pyrophosphoramide, O((*i*PrNH)$_2$PO)$_2$ **1** has been determined from single-crystal X-ray diffraction data while the chemical identity of the species was supported by IR, ^{1}H NMR, ^{31}P NMR, and GC MS data (see SI). A thorough structural comparison of **1** with other pyrophosphoramides for which the crystal structures have been published previously was carried out. **1** forms a novel supramolecular motif previously unattested for mono-N-substituted pyrophosphoramides. This motif was composed of two different synthons with P=O···H–N interactions. The great impact of this type of hydrogen bonding on the supramolecular motifs in all previously published mono-N-substituted pyrophosphoramides could be confirmed also for **1**. Trends regarding the effects of the various organic moieties within the different compounds were difficult to describe due to the lack of systematic data. No comparison of **1** with the di-N-substituted pyrophosphoramides was undertaken, given that the trends in packing are significantly different between this group and the mono-N-substituted pyrophosphoramides.

The differences observed between the supramolecular motifs present in **1** and the supramolecular features of other mono-N-substituted pyrophosphoramides indicate that there are possibly other supramolecular motifs that have not yet been discovered yet. The crystal structure of **1** further expands the diversity of possible supramolecular synthons.. The different synthon in **1** ($R_2^1(8)$ ring), not known in previously described mono-N-substituted pyrophosphoramides, adds a new strong structural motif to the viable synthons known experimentally for mono-N-substituted pyrophosphoramides. It can also be considered to be a viable option for the discovery of new co-crystals of these

species [20,21]. Different solid-state forms of pyrophosphoramides as well as co-crystals formed with other organic and inorganic species will have different physical properties and, at times different chemical properties compared to the currently marketed compounds without changing the actual molecule [26–30]. This is important for mono-N-substituted pyrophosphoramides given their possible use as a pesticide. The formation of different forms with different thermodynamic and kinetic stabilities can aid in complexation reactions and e.g., diminish decomposition on storage, a property of great importance for use in agriculture [28,29,31,32].

However, given the disparity between the various experimental techniques used in both the structures described in the literature and the current study further work at different temperatures, including X-ray data from powders, must be undertaken to obtain a more comprehensive understanding of the relationship between the chemical and physical properties and the crystal structures of various pyrophosphoramides.

Supplementary Materials: The following are available online at www.mdpi.com//3/1/13/s1. Interpretation of IR, NMR and mass spectra. Figure S1: IR spectrum of $O((i\text{PrNH})_2PO)_2$. Figure S2: IR spectrum of $O((i\text{PrNH})_2PO)_2$ obtained from column chromatography. Figure S3: ^1H NMR spectrum of $O((i\text{PrNH})_2PO)_2$. Figure S4: ^1H NMR spectrum of $O((i\text{PrNH})_2PO)_2$ from column chromatography. Figure S5: $^{31}P\{^1H\}$ NMR spectrum of $O((i\text{PrNH})_2PO)_2$. Figure S6: $^{31}P\{^1H\}$ NMR spectrum of $O((i\text{PrNH})_2PO)_2$ from column chromatography. Figure S7: Gas chromatograph of $O((i\text{PrNH})_2PO)_2$. Figure S8: Gas chromatograph of $O((i\text{PrNH})_2PO)_2$ from column chromatography. Figure S9: Mass spectrum of $O((i\text{PrNH})_2PO)_2$ from column chromatography. Table S1: ^1H NMR experimental data and assignment for proton peaks of $O((i\text{PrNH})_2PO)_2$ in $CDCl_3$. Table S2: ^1H NMR experimental data and assignment for proton peaks of $O((i\text{PrNH})_2PO)_2$ from column chromatography in $CDCl_3$. Table S3: Mass spectra peak data for the $O((i\text{PrNH})_2PO)_2$ Gas chromatography peaks at 6.618 and 7.313 min.

Author Contributions: Conceptualization, D.M. U.B. and L.V.-Z.; Methodology and Practical Chemical and Spectroscopic studies, D.M.; XRD data collection and structure solution, U.B.; Writing—original draft preparation, D.M.; Writing—review and editing, U.B. and L.V.-Z.; Project administration, U.B. and L.V.-Z.; funding acquisition, L.V.-Z and U.B. All authors have read and agreed to the published version of the manuscript.

Funding: The research work disclosed in this publication is partially funded by the Endeavour Scholarship Scheme (Malta). Scholarships are part-financed by the European Union—European Social Fund (ESF)—Operational Programme II—Cohesion Policy 2014–2020 "Investing in human capital to create more opportunities and promote the well-being of society". It was also funded by by the project: "Setting up of transdisciplinary research and knowledge exchange (TRAKE) complex at the University of Malta (ERDF.01.124)", which is being co-financed through the European Union through the European Regional Development Fund 2014–2020 (L.V.-Z. and U.B.).

Data Availability Statement: The data presented in this study are available in the supplementary materials.

Acknowledgments: The authors would like to thank Robert M. Borg for his contribution regarding NMR data collection and analysis and Godwin Sammut for his contribution in GC MS data collection, both of the Department of Chemistry, Faculty of Science, University of Malta. We would also like to thank Jens Meyer from STOE & Cie GmbH for his contribution in SXRD data collection.

Conflicts of Interest: The authors declare no conflict of interest.

Appendix A

Appendix A.1. Single Crystal X-Ray Diffraction Experimental Description

Single crystals of $C_{12}H_{32}N_4O_3P_2$ [$O(i\text{PrNH})_2PO)_2$] were [Layering $CHCl_3$ solution with 30–40 petroleum ether]. A suitable crystal was selected and [Collected in oil and frozen] on a STOE STADIVARI diffractometer. The crystal was kept at 293 K during data collection. Using Olex2 [1], the structure was solved with the ShelXT [2] structure solution program using Intrinsic Phasing and refined with the ShelXL [3] refinement package using Least Squares minimisation. CCDC 2055906 contains the supplementary

crystallographic data for this paper. The data can be obtained free of charge from The Cambridge Crystallographic Data Centre via www.ccdc.cam.ac.uk/structures.

1. Dolomanov, O.V., Bourhis, L.J., Gildea, R.J, Howard, J.A.K. & Puschmann, H. (2009), J. Appl. Cryst. 42, 339–341.
2. Sheldrick, G.M. (2015). Acta Cryst. A71, 3–8.
3. Sheldrick, G.M. (2015). Acta Cryst. C71, 3–8.

Crystal structure determination of [O(*i*PrNH)$_2$PO)$_2$]

Crystal Data for $C_{12}H_{32}N_4O_3P_2$ (M = 342.35 g/mol): orthorhombic, space group *Pca*2$_1$ (no. 29), a = 20.342(2) Å, b = 5.0495(6) Å, c = 19.103(3) Å, V = 1962.2(4) Å^3, Z = 4, T = 295 K, μ(CuKα) = 2.133 mm^{-1}, *Dcalc* = 1.159 g/cm^3, 43032 reflections measured (8.696° ≤ 2Θ ≤ 137.27°), 3317 unique (R_{int} = 0.0557, R_{sigma} = 0.0226) which were used in all calculations. The final R_1 was 0.0408 (I > 2σ(I)) and wR_2 was 0.1075 (all data).

Appendix A.2. Refinement Model Description

Number of restraints—1, number of constraints—unknown.
Details:
1. Fixed Uiso

- At 1.2 times of all C(H) groups
- At 1.5 times of all CH_3 groups

2. a Ternary CH refined with riding coordinates: C10(H10), C20(H20), C30(H30), C40(H40)

2. b Idealised Me refined as rotating group: C31(H31A,H31B,H31C), C11(H11A,H11B,H11C), C41(H41A,H41B,H41C), C42(H42A,H42B, H42C), C12(H12A,H12B,H12C), C22(H22A,H22B,H22C), C32(H32A,H32B,H32C), C21(H21A, H21B,H21C)

References

1. Li, B.; Stribley, J.A.; Ticu, A.; Xie, W.; Schopfer, L.M.; Hammond, P.; Brimijoin, S.; Hinrichs, S.H.; Lockridge, O. Abundant Tissue Butyrylcholinesterase and Its Possible Function in the Acetylcholinesterase Knockout Mouse. *J. Neurochem.* **2002**, *75*, 1320–1331, doi:10.1046/j.1471-4159.2000.751320.x.
2. Pohanka, M. Cholinesterases, a target of pharmacology and toxicology. *Biomed. Pap.* **2011**, *155*, 219–223, doi:10.5507/bp.2011.036.
3. Lickerish, L.A. Studies on commercial octamethylpyrophosphor- amide (schradan) V.*-Insecticidal Comparisons of the Two Main Constituents. *J. Sci. Food Agric.* **1953**, *4*, 24–28.
4. Rediske, J.H.; Lawrence, W.H. Octamethylpyrophosphoramide (OMPA) As a Systemic Animal Repellent for Douglas-Fir Seedlings. *For. Sci.* **1964**, *10*, 93–103.
5. Joesten, M.D. The donor properties of pyrophosphate derivatives. V. Complexes of molybdenum (V) oxychloride, uranyl ion, and thorium (IV) ion with octamethylpyrophosphoramide. *J. Inorg. Nucl. Chem.* **1967**, *6*, 1598–1599.
6. du Preez, J.G.H.; Sadie, F.G. Hexamethylphosphoramide and octamethylpyrophosphoramide complexes of tetravalent metal chlorides. *J. S. Afr. Chem. Inst.* **1966**, *19*, 73–84.
7. Joesten, M.D.; Hussain, M.S.; Lenhert, P.G. Structure studies of pyrophosphate chelate rings. I. Crystal structures of tris-octamethylpyrophosphoramide complexes of cobalt (II), magnesium (II), and copper (II)perchlorates. *Inorg. Chem.* **1970**, *9*, 151–161, doi:10.1021/ic50083a031.
8. Hussain, M.S.; Joesten, M.D.; Lenhert, P.G. Structuee Studies of Pyrophosphate Chelate Rings. II. The Crystal Structuee of Bis(Perchlorato)Bis(Octamethylpyrophosphoramide)Copper(II). *Inorg. Chem.* **1970**, *9*, 162–168.
9. Kepert, D.L.; Patrick, J.M.; White, A.H. Structure and Stereochemistry in f-Block Complexes of High Co-Ordination Number. Part 3.* The [M(Bidentate Ligand)2(Unidentate Ligand)4] System: Crystal Structures of Tetrakis (Isothiocyanato)-Bis(Octamethylpyrophosphoramide. *Dalton Trans.* **1983**, *0*, 559–566.
10. Cameron, T.S.; Cordes, R.E.; Jackman, F.A. Synthesis and Crystal Structure of μ-Oxo-bis(phosphenyl-ortho-toluidide). *Z. Nat. B* **1978**, *33*, 728–730, doi:10.1515/znb-1978-0708.
11. Pourayoubi, M.; Padělková, Z.; Rostami Chaijan, M.; Růžička, A. N,N′,N″,N‴-Tetrakis(2-Methylphenyl)-Oxybis(Phosphonic Diamide): A Redetermination at 150 K with Mo K Radiation. *Acta Crystallogr. Sect. E Crystallogr. Commun.* **2011**, *67*, 466–470.
12. Pourayoubi, M.; Tarahhomi, A.; Karimi Ahmadabad, F.; Fejfarová, K.; Lee, A. Van Der; Dušek, M. Two New XP(O)[NHC(CH3)3]2 Phosphor-Amidates, with X = (CH3)2N and [(CH3)3CNH]2P(O)(O). *Acta Crystallogr. Sect. C Cryst. Struct. Commun.* **2012**, *68*, 164–169.
13. Tarahhomi, A.; Pourayoubi, M.; Golen, J.A.; Zargaran, P.; Elahi, B.; Rheingold, A.L.; Ramírez, M.A.L.; Percino, T.M. Hirshfeld surface analysis of new phosphoramidates. *Acta Crystallogr. Sect. B Struct. Sci. Cryst. Eng. Mater.* **2013**, *69*, 260–270, doi:10.1107/s2052519213009445.

14. Giffin, N.A.; Hendsbee, A.D.; Roemmele, T.L.; Lumsden, M.D.; Pye, C.C.; Masuda, J.D. Preparation of a Diphosphine with Persistent Phosphinyl Radical Character in Solution: Characterization, Reactivity with O2, S8, Se, Te, and P4, and Electronic Structure Calculations. *Inorg. Chem.* **2012**, *51*, 11837–11850, doi:10.1021/ic301758k.
15. Yerramsetti, N.; Unruh, D.K.; Li, G. CCDC 1559159: Experimental Crystal Structure Determination. https://www.ccdc.cam.ac.uk/structures/search?id=doi:10.5517/ccdc.csd.cc1pbfgx&sid=DataCite (accessed on 28 June 2017)
16. Tarahhomi, A.; Pourayoubi, M.; Fejfarová, K.; Dusek, M. A Novel Amido-pyrophosphate MnII Chelate Complex with the Synthetic Ligand O{P(O)[NHC(CH3)3]2}2(L): [Mn(L)2{OC(H)N(CH3)2}2]Cl2.2H2O. *Acta Crystallogr. Sect. C Struct. Chem.* **2013**, *69*, 225–229.
17. Desiraju, G.R. Supramolecular Synthons in Crystal Engineering—A New Organic Synthesis. *Angew. Chem. Int. Ed.* **1995**, *34*, 2311–2327, doi:10.1002/anie.199523111.
18. Desiraju, G.R. Designer Crystals: Intermolecular Interactions, Network Structures and Supramolecular Synthons. *Chem. Commun.* **1997**, *16*, 1475–1482.
19. Desiraju, G.R. Hydrogen Bridges in Crystal Engineering: Interactions without Borders. *Acc. Chem. Res.* **2002**, *35*, 565–573, doi:10.1021/ar010054t.
20. Desiraju, G.R. Crystal Engineering: A Holistic View. *Angew. Chem. Int. Ed.* **2007**, *46*, 8342–8356, doi:10.1002/anie.200700534.
21. Desiraju, G.R. Crystal engineering: A brief overview. *J. Chem. Sci.* **2010**, *122*, 667–675, doi:10.1007/s12039-010-0055-2.
22. Goehring, M.; Niedenzu, K. Diphosphorsäure-tetrakis-dimethylamid. *Angew. Chem.* **1956**, *68*, 704, doi:10.1002/ange.19560682206.
23. Dolomanov, O.V.; Bourhis, L.J.; Gildea, R.J.; Howard, J.A.K.; Puschmann, H. OLEX2: A complete structure solution, refinement and analysis program. *J. Appl. Crystallogr.* **2009**, *42*, 339–341, doi:10.1107/s0021889808042726.
24. *ACD/ChemSketch*; Advanced Chemistry Development: Toronto, ON, Canada, 2013.
25. Macrae, C.F.; Bruno, I.J.; Chisholm, J.A.; Edgington, P.R.; McCabe, P.; Pidcock, E.; Rodriguez-Monge, L.; Taylor, R.J.; Van De Streek, J.; Wood, P.A. Mercury CSD 2.0—New features for the visualization and investigation of crystal structures. *J. Appl. Crystallogr.* **2008**, *41*, 466–470, doi:10.1107/s0021889807067908.
26. Bernstein, J.; Sheva, B. Pinching Polymorphs. *Nat. Mater.* **2005**, *4*, 427–429.
27. Haleblian, J.; McCrone, W. Pharmaceutical Applications of Polymorphism. *J. Pharm. Sci.* **1969**, *58*, 911–929, doi:10.1002/jps.2600580802.
28. De Villiers, M.; Van Der Watt, J.; Lötter, A. Kinetic study of the solid-state photolytic degradation of two polymorphic forms of furosemide. *Int. J. Pharm.* **1992**, *88*, 275–283, doi:10.1016/0378-5173(92)90325-v.
29. Foltz, M.F.; Coon, C.L.; Garcia, F.; Nicholas, A.L., III. The Thermal Stability of the Polymorphs of Hexanitrohexaazaisowurtzitane. *Part I Propellants Explos. Pyrotech.* **1994**, *19*, 19–25.
30. Hilfiker, R.; Blatter, F.; Von Raumer, M. Relevance of Solid-state Properties for Pharmaceutical Products. In *Polymorphism*; Wiley: Hoboken, NJ, USA, 2006; pp. 1–19.
31. Haywood, A.; Mangan, M.; Grant, G.; Glass, B. Extemporaneous Isoniazid Mixture: Stability Implications. *J. Pharm. Pr. Res.* **2005**, *35*, 181–182, doi:10.1002/j.2055-2335.2005.tb00333.x.
32. Sarcevica, I.; Orola, L.; Veidis, M.V.; Podjava, A.; Belyakov, S. Crystal and Molecular Structure and Stability of Isoniazid Cocrystals with Selected Carboxylic Acids. *Cryst. Growth Des.* **2013**, *13*, 1082–1090, doi:10.1021/cg301356h.